

1

Revision 3

2

Aluminum ion occupancy in the structure of synthetic saponites: effect on

3

crystallinity

4

5

Hongping He^{1,*}, Tian Li^{1,2}, Qi Tao¹, Tianhu Chen³, Dan Zhang^{1,2}, Jianxi Zhu¹, Peng

6

Yuan¹ and Runliang Zhu¹

7

8

¹ Key Laboratory of Mineralogy and Metallogeny, Guangzhou Institute of Geochemistry,

9

Chinese Academy of Sciences, 510640, China

10

² University of Chinese Academy of Sciences, Beijing 100049, China

11

³ School of Natural Resources and Environment, Hefei University of Technology, Hefei

12

230009, China

13

14 *** Corresponding author:**

15

Dr. Hongping He

16

Present address: Guangzhou Institute of Geochemistry, Chinese Academy of Sciences,

17

No. 511 Kehua Street, Guangzhou, 510640.

20

E-mail address: hehp@gig.ac.cn

21 **ABSTRACT**

22 Two series of saponites with fixed (Si+Al)/Mg and Si/Mg ratios, respectively, were
23 synthesized by using hydrothermal methods. The obtained products were characterized
24 by XRD, XRF, ^{27}Al and ^{29}Si MAS NMR, SEM and TEM. XRD patterns showed that
25 well-ordered saponites were obtained in the initial Si/Al ratio range of 5.43 – 7.89.
26 Beyond this Si/Al ratio range, poorly crystallized saponites were obtained with small
27 crystallized particles, which can be seen from TEM images. When intercalating saponite
28 with surfactant, the intercalated products displayed strong and well-ordered (00l)
29 reflections, indicating that layered saponite has been successfully synthesized in the
30 present study. ^{27}Al MAS NMR spectra demonstrated that well crystallized synthetic
31 saponites had a higher Al(IV)/Al(VI) ratio than the poorly crystallized samples, which is
32 an important factor affecting the crystallinity of synthetic saponite. A one-to-one
33 substitution (i.e. $1 \text{ Al}^{3+} \rightarrow 1 \text{ Mg}^{2+}$) actually occurred in the octahedral sheet and this
34 substitution had a negative effect on the crystallinity of the synthetic saponites. After
35 grafting the synthetic saponites with silane, the decreased intensity of the ^{29}Si NMR
36 signal at -86 ppm and the increased intensity of $\text{Q}^3 \text{ Si}(0\text{Al})$ and $\text{Q}^3 \text{ Si}(1\text{Al})$ signals
37 strongly suggested that the signal at ca. -86 ppm corresponded to $\text{Q}^2 \text{ Si}$ at the layer edges
38 of saponite.

39 **Keywords:** Synthetic saponite, occupancy of aluminum ion, crystallinity, ^{27}Al and ^{29}Si
40 MAS NMR, isomorphous substitution

41 **INTRODUCTION**

42 Saponite is a 2:1 type trioctahedral phyllosilicate of the smectite group of clay minerals.
43 The saponite structure is composed of a central octahedral sheet with essentially a brucite
44 $[\text{Mg}_3(\text{OH})_6]$ structure, in which four out of six OH^- groups are replaced by oxygen atoms.
45 These oxygen atoms are connected to two tetrahedral sheets consisting of Si^{4+} and O^{2-}
46 situated on both sites of the central octahedral sheet. The ideal structural formula of
47 saponite can be presented as $\text{M}_x^+[\text{Mg}_3][\text{Si}_{4-x}\text{Al}_x]\text{O}_{10}(\text{OH})_2 \cdot n\text{H}_2\text{O}$, where M is the
48 exchangeable interlayer cation (Brigatti et al. 2006).

49 Natural saponites are usually formed from weathering of Mg-containing rocks. Due to
50 the complexities of the chemical compositions of the mother rocks and physical-chemical
51 conditions in the geological process of saponite formation, isomorphous substitution of
52 Al^{3+} for Si^{4+} in the tetrahedral sheet and Mg^{2+} by metals with different valencies (e.g.,
53 Al^{3+} , Fe^{3+} , Li^+ , Mn^{2+} , Ni^{2+} , Zn^{2+}) in the octahedral sheet extensively occurred (Mackenzie
54 1957; Vicente Rodriguez et al. 1994). Generally, the isomorphous substitution of Al^{3+} for
55 Si^{4+} in the tetrahedral sheet is dominant and saponite is negatively charged, in which the
56 net negative charges are compensated by exchangeable interlayer cations.

57 Because of its high surface acidity and thermal stability, saponite has been widely used
58 as a heterogeneous catalyst and catalyst support (Varma 2002; Casagrande et al. 2005;
59 Vogels et al. 2005a) as well as a filler in the preparation of polymer nanocomposites
60 (Giannelis et al. 1999; Alexandre and Dubois 2000; Zanetti et al. 2000). The surface
61 properties (e.g., acidity, interlayer swelling) of clay minerals are also highly dependent on

62 their chemical composition which, in turn, is strongly affected by the extent of
63 isomorphous substitution in their layer structure (Moronta, 2004).

64 For industrial applications, it is very important that the composition and properties of
65 clay materials can be adjusted for different industries. But for a specific field, the
66 composition and property are demanded to be homogeneous. The chemical composition
67 and property of natural saponites can be extremely variable, which strongly depend on
68 the chemical composition of the mother rock, the genesis process and the provenance
69 (Utracki et al. 2007). This variability represents a strong limitation in their applications
70 especially when surface properties have to be strictly controlled, such as in catalysis.

71 For this reason, different methods have been developed to prepare synthetic saponites
72 with well-controlled chemical composition and property (Farmer et al. 1991, 1994;
73 Klopogge et al. 1993, 1994a, 1994b; Vogels et al. 1997, 2005b; Kawi and Yao 1999;
74 Yao et al. 2005; Higashi et al. 2007; Bisio et al. 2008; Vicente et al. 2010; Xue and
75 Pinnavaia 2010). For instance, Farmer et al. (1991, 1994) synthesized well-formed
76 saponite in hydrazine-water mixtures and found that the presence of Fe^{2+} in a calcareous
77 environment may promote the formation of saponite. Different NH_4^+ saponites with
78 variable crystallinity, platelet dimensions, specific surface areas and cation exchange
79 capacities were obtained by varying synthesis gel composition and crystallization
80 temperature (Klopogge et al. 1993). Bisio et al. (2008) reported that different $\text{H}_2\text{O}/\text{Si}$
81 molar ratios of the gels strongly affected the surface properties of the saponite samples,
82 including texture, adsorption property, thermal stability, and acidity of surface species.

83 These studies paid attention mainly to the influences of experimental conditions on the
84 crystallinity and properties of synthetic saponites (Zhang et al. 2010).

85 In addition to the effects of synthesis conditions (e.g., starting materials, temperature,
86 pressure, ageing time, microwave heating) (Kloprogge et al. 1999; Zhang et al. 2010), a
87 noteworthy problem is the occupancy of the substituting ions (e.g., Al^{3+}) in synthetic
88 saponites, which is the key factor controlling the structure and properties of synthetic
89 saponites. Isomorphous substitution will lead to a distortion of tetrahedral and octahedral
90 sheets and a further effect on the stacking order of saponite layers (Kloprogge et al.
91 1994a). On the other hand, different types of substitution can result in a significant effect
92 on net charges of synthetic saponites and a further effect on cation exchange capacity
93 (CEC). For example, a muscovite substitution in the octahedral sheet (Vogels et al.
94 2005b), $2\text{Al}^{3+} + 1 \text{vacancy} \rightarrow 3\text{Mg}^{2+}$, has no effect on the total net charges of saponite
95 whereas a one-to-one ($1 \text{Al}^{3+} \rightarrow 1 \text{Mg}^{2+}$) substitution will create a positive charge
96 (Suquet et al. 1981). The latter compensates a negative charge created by the substitution
97 of Si^{4+} by Al^{3+} in the tetrahedral sheet and decreases the total net charge of saponite.

98 In this respect, Kloprogge and co-workers have conducted a series of investigations
99 during the last two decades, by using a combination of various characterization
100 techniques (Kloprogge et al. 1993, 1994a, 1994b; Vogels et al. 1997, 2005b). Al ions
101 could occupy both tetrahedral and octahedral sites and the Al(IV)/Al(VI) ratio increased
102 with increasing synthesis temperature (Kloprogge et al. 1994a, 1994b). A muscovite
103 substitution ($2\text{Al}^{3+} + \text{vacancy} \rightarrow 3\text{Mg}^{2+}$) was proposed for the substitution of Al^{3+} for

104 Mg^{2+} in the octahedral sheet of synthetic saponites (Vogels et al. 2005b). This is very
105 different from the model ($1 Al^{3+} \rightarrow 1 Mg^{2+}$) suggested by Suquet et al. (1981). These
106 findings are helpful for understanding the structure and property of synthetic saponites.
107 Unfortunately, further investigation about the relationship between the occupancy of the
108 substituting Al^{3+} and the structure/property of synthetic saponite has not been reported so
109 far.

110 The main aim of this study is to investigate occupancy priority of Al ions between
111 tetrahedral and octahedral sites and its effect on the structure and crystallinity of synthetic
112 saponites. Hence, two series of saponites with fixed (Si+Al)/Mg and Si/Mg ratios,
113 respectively, were synthesized by using hydrothermal methods as described by Kawi and
114 Yao (1999). The obtained saponites were characterized by X-ray diffraction (XRD),
115 X-ray fluorescence spectroscopy (XRF), ^{27}Al and ^{29}Si solid-state magic-angle-spinning
116 nuclear magnetic resonance spectroscopy (MAS NMR), scanning electron microscopy
117 (SEM) and transmission electron microscopy (TEM).

118 **EXPERIMENTAL METHODS**

119 **Preparation methods**

120 **Synthesis of saponite.** Synthetic saponite samples were prepared by modifying the
121 literature method indicated by Kawi and Yao (1999). The ratios of Si, Al and Mg in the
122 starting materials and the products are shown in Table 1. A general synthesis procedure is
123 as follows: A buffer solution was prepared by dissolving 18.00 g of NaOH and 32.80 g of
124 $NaHCO_3$ in 250 mL of deionized water. Then, desired amounts of sodium metasilicate

125 (Na₂SiO₃·9H₂O) solution were added to the buffer solution under vigorous stirring. The
126 obtained solution was noted as Solution A. Solution B was prepared by dissolving desired
127 amounts of AlCl₃·6H₂O and 30.80 g of MgCl₂·6H₂O in 25 mL of deionized water. Then,
128 Solution B was slowly added into Solution A with continuous stirring until a uniform gel
129 was eventually obtained. After that, the gel was transferred to a Teflon-lined autoclave
130 and treated at 160 °C for 24 h.

131 In order to exclude the excess electrolytes in the resultant products, the obtained
132 products were washed 8 times with deionized water, then dried at 80 °C and ground
133 before characterizations. The series of synthetic saponites with fixed (Si+Al)/Mg (Series I)
134 was prepared by adjusting the amounts of AlCl₃·6H₂O and Na₂SiO₃·9H₂O, and the
135 obtained products were denoted as SAP-I-X, in which X stands for Si/Al ratio in the
136 starting material. By the same method, the synthetic saponites with fixed Si/Mg (Series II)
137 were prepared by adjusting the added amounts of AlCl₃·6H₂O. The obtained products
138 were marked as SAP-II-X (X = Si/Al ratio in the starting material). The cationic
139 exchange capacity (CEC) of the synthesized saponites was determined by the method
140 reported in the literature (Hu et al. 2000; Bisio et al. 2008). The synthetic saponites (500
141 mg) were exchanged with 30 mL of a 0.05 M solution of [Co(NH₃)₆]³⁺. After separation
142 by centrifugation, the solution was analyzed by UV–Vis spectrophotometer (UV-7504).
143 The decrease of absorbance at 474 nm, typical of the CT transition of [Co(NH₃)₆]³⁺, is
144 quantitatively related to the difference in concentration by means of a calibration with
145 standard solutions.

146 **Intercalating saponite with surfactant.** Intercalation experiments were carried out
147 with hexadecyltrimethylammonium bromide (HDTMAB) at a concentration to yield an
148 amount equivalent to the CEC of the saponite as described in the literature (He et al.
149 2010). A desired amount of HDTMAB was dissolved in 30 mL of distilled water. Then,
150 1.00 g of synthetic saponite (e.g., SAP-I-2.33, SAP-I-5.43, SAP-I-7.89) was added into
151 the prepared solution containing HDTMAB. The mixtures were stirred at 60 °C for 6 h.
152 All the products were washed with deionized water six times and dried at 80 °C. The
153 intercalated products prepared from SAP-I-2.33, SAP-I-5.43 and SAP-I-7.89 were
154 marked as SAP-I-2.33-1CEC, SAP-I-5.43-1CEC and SAP-I-7.89-1CEC, respectively.

155 **Grafting saponite with silane.** The grafting reaction was carried out in a mixture of
156 water/ethanol (25/75 by volume) as reported in the literature (He et al. 2005). 3.00 g of
157 synthetic saponite (SAP-I-5.43, SAP-I-12.30 and SAP-I-39.00) and 7.05 mL of
158 3-aminopropyltriethoxysilane (APTES, with a purity of 99%, from Aldrich) were mixed
159 by stirring in 60 mL of water/ethanol mixture at 80 °C for 24 h. The products were
160 filtered, washed six times using the mixture of water/ethanol and dried at 80 °C. Then, the
161 resultant product was grounded and placed in a sealed container for characterization. The
162 grafting products prepared from SAP-I-5.43, SAP-I-12.30 and SAP-I-39.00 were denoted
163 as SAP-I-5.43-APTES, SAP-I-12.30-APTES and SAP-I-39.00-APTES, respectively.

164 **Analytical techniques**

165 **X-ray diffraction (XRD).** Randomly oriented powder X-ray diffraction patterns
166 (XRD), to determine the basal spacing of the sample, were collected between 1° and 80°

167 (2 θ) at a scanning rate of 1° (2 θ) min⁻¹ on a Bruker D8 Advance diffractometer with
168 Ni-filtered CuK α radiation (λ =0.154 nm, 40 kV and 40 mA).

169 **Transmission electron microscopy (TEM).** TEM images were collected on a JEOL
170 2010 high resolution transmission electron microscope operated at an accelerating
171 voltage of 200 kV. Specimens were prepared by dispersing the sample in ethanol and
172 ultrasonically treating for 5 minutes. A drop of the resultant suspension was placed on a
173 holey carbon film supported by a copper grid, after which the ethanol was evaporated.
174 Chemical analysis was executed using the attached energy-dispersive X-ray (EDX)
175 analyzer to obtain the molar ratio of Si, Al and Mg in the synthetic saponites.

176 **Field Emission Scanning Electron Microscopy (FE-SEM).** SEM images were
177 recorded on a Sirion-200 field emission scanning electron microscope, using a tungsten
178 filament as electron source. Samples were disaggregated by sonication in ethanol. A
179 conductive coating of gold by low-pressure plasma was finally deposited to avoid the
180 electronic charging on the insulating particles under the electron beam.

181 **X-ray fluorescence spectroscopy (XRF).** Elemental analysis was conducted on a
182 Rigaku RIX 2000 X-ray fluorescence spectrometer (XRF). Saponite samples were
183 ground using an agate mortar to 200 mesh. Loss-on-ignition was obtained by weight loss
184 of the sample ignited in a furnace at 900 °C for 2 h and allowed to cool in a desiccator to
185 minimize moisture absorption. About 500 mg calcined saponite sample and 4 g Li₂B₄O₇
186 were mixed homogeneously, and the mixture was digested in a Pt-Au alloy crucible at
187 1150 °C in a high-frequency furnace. The quenched bead was used for XRF

188 measurements (Goto and Tatsumi 1994). The calibration line for Si/Al ratio used in
189 quantification was produced by bivariate regression of the Si/Al data measured for 36
190 reference materials encompassing a wide range of silicate compositions, and analytical
191 uncertainties were mostly between 1% and 5%.

192 **Magic-angle-spinning nuclear magnetic resonance spectroscopy (MAS NMR).**

193 Both ^{27}Al MAS NMR and ^{29}Si cross polarization (CP) MAS NMR measurements were
194 carried out on a Bruker AVANCE III 400 WB spectrometer. The resonance frequency of
195 ^{29}Si was 79.5 MHz. Samples were packed in a 7 mm ZrO_2 rotor and spun at the magic
196 angle (54.7°), and the spin rate was 7 kHz. ^{29}Si CPMAS NMR spectra were recorded with
197 a contact time of 4.5 ms and a recycle delay of 2 s, using tetramethylsilane (TMS) as an
198 external reference. The corresponding resonance frequency of ^{27}Al was 104.3 MHz.
199 Samples were packed in a 4 mm ZrO_2 rotor and spun at the magic angle (54.7°), and the
200 spin rate was 15 kHz. Single pulse magic angle spinning spectra were acquired using a
201 high power $0.5\ \mu\text{s}$ pulse, corresponding to a tip angle of 18° and a recycle delay of 0.5 s.
202 The ^{27}Al chemical shift was externally referenced to a 1.0 M aqueous solution of
203 $\text{Al}(\text{NO}_3)_3$. Peak component analysis was undertaken using a Gauss–Lorentz cross-product
204 function applied by the PEAKFIT software package. The minimum number of
205 component bands was obtained with squared correlations ≥ 0.995 .

206 **RESULTS AND DISCUSSION**

207 **Crystallinity and morphology of the synthetic saponites**

208 Table 1 shows the molar ratios of Si, Al and Mg in the synthesis gels, CEC and

209 Al(IV)/Al(VI) ratios of the synthesized saponites. In the case of Series I, the added
210 amount of Mg and the total amount of Si and Al were fixed (i.e., (Si+Al):Mg = 4:3) while
211 the Si/Al ratio was different from each other. For Series II, the added Si and Mg amounts
212 were fixed and that of Al was varied, keeping an identical Si/Al ratio to that of the
213 corresponding one in Series I. That is to say, samples in Series II can be considered as a
214 case in which the added Mg amount was changed while the Si/Al ratio was identical to
215 the corresponding one in Series I. This is helpful for us to well understand the influence
216 of the added amount of Mg on the occupancy of Al in the synthetic saponites. As shown
217 in Table 1, the nominal Si/Al ratios are similar to those measured, implying that the
218 synthesis reaction is almost complete.

219 The powder XRD patterns of the synthetic saponites are shown in Figure 1. A series of
220 reflections are recorded at ca. 1.33-1.41, 0.45-0.46, 0.26 and 0.153 nm, corresponding to
221 (001), (02,11), (13,20) and (060) reflections of the synthetic products, respectively
222 (Vogels et al. 2005b). The d value of (006) reflection at 0.153 nm is an indicative
223 evidence for trioctahedral clay minerals. There were no obvious reflections of impurities,
224 indicating that pure saponites have been successfully synthesized. However, the broad
225 and weak (001) reflections suggest that the crystallinity of the synthetic saponites is
226 relatively poor when compared with natural ones.

227 XRD patterns (Fig. 1) show that relatively strong (001) reflections were recorded in
228 SAP-I-7.89, SAP-I-5.43 and SAP-I-4.50 in Series I, and SAP-II-7.89 and SAP-II-5.43 in
229 Series II, indicating that well crystallized and ordered saponites were synthesized. With

230 an increase or decrease of Si/Al ratio, the (001) reflection was obviously weakened and
231 broadened, corresponding to poorly crystallized synthetic saponites. However,
232 considering the added amount of Mg in Series II is significantly more than that in the
233 corresponding sample in Series I (Table 1), we can conclude that the initial Si/Al ratio has
234 a more prominent effect on the crystallinity of the synthetic saponites than Mg does.

235 This is also evidenced by SEM and TEM observations as shown in Figure 2. In the
236 SEM images of SAP-I-5.43 (Fig. 2b) and SAP-I-7.89 (Fig. 2c), well crystallized layers of
237 saponites can be extensively observed. However, SAP-I-2.33 (Fig. 2a) and SAP-I-39.00
238 (Fig. 2d) displayed small particle aggregates and some discrete small saponite layers
239 could be observed among particles in SAP-I-39.00. As further indicated by TEM images,
240 the aggregated particles in SAP-I-2.33 (Fig. 2e) contained crystallized small saponite
241 layers with random orientation while SAP-I-5.43 (Fig. 2f) displayed large saponite layers.
242 A small amount of amorphous materials, as determined by selected area electron
243 diffraction (SAED), were indeed observed in the synthetic saponites. The Si/Al ratios in
244 SAP-I-2.33, SAP-I-5.43 and SAP-I-7.89, derived from energy-dispersive X-ray (EDX)
245 analysis, are ca. 2.4 (average of nine points), 5.9 (average of five points) and 8.1 (average
246 of six points), respectively. These values are comparable to those determined using X-ray
247 fluorescence (XRF) as shown in Table 1.

248 To further identify the successful synthesis of saponites, intercalation experiments
249 with hexadecyltrimethylammonium bromide (HDTMAB) were conducted at a
250 concentration to yield an amount equivalent to the CEC of the saponite and the XRD

251 patterns of the intercalated products are shown in Figure 3. A strong and well ordered
252 (001) reflection with a basal spacing at ca. 2.24 nm for SAP-I-2.33-1CEC (Fig. 3b), 2.83
253 nm for SAP-I-5.43-1CEC (Fig. 3d), 2.32 nm for SAP-I-7.89-1CEC (Fig. 3f) were
254 recorded, reflecting a paraffin bilayer arrangement adopted by the intercalated surfactant
255 within the interlayer space. This is similar to HDTMAB modified 2:1 type clay minerals
256 reported in the literature (Lagaly et al. 1981; He et al. 2004). Interestingly, even those
257 poorly crystallized synthetic saponites (e.g. SAP-I-2.33) displayed a (001) reflection with
258 high intensity after intercalation with surfactant. The intercalation experiments clearly
259 showed that layered saponites have been successfully synthesized in this study.

260 As discussed above, both XRD and electron microscope analysis results showed that
261 saponites have been successfully synthesized and the initial Si/Al ratio is an important
262 factor affecting the order of lamellae stacking and the particle size of the synthetic
263 saponites (Costenaro et al. 2012). This is associated with the distortion extent of the
264 structural units due to the isomorphous substitutions of Al^{3+} for Mg^{2+} in the octahedral
265 sheet and Al^{3+} for Si^{4+} in the tetrahedral sheet.

266 From Table 1, we can find that the measured Si/Al ratio in the synthetic products of
267 Series II was higher than that in the corresponding samples of Series I, due to a larger
268 added amount of Mg in the starting materials of Series II. As Mg only occupies the
269 octahedral sites in the saponite structure, the difference of the measured Si/Al ratio
270 implies that there is an occupancy competition between Al and Mg, and Mg can readily
271 enter into the octahedral sites prior to Al. This leads to a significant influence on the

272 occupancy of Al ions in octahedral and tetrahedral sites in the saponite structure, which is
273 further supported by MAS NMR spectra (see below).

274 **Occupancy of Al ions in the synthetic saponites**

275 The information about Al occupancy in the synthetic saponites can be obtained from
276 the ^{27}Al MAS NMR spectra (Figs. 4A and 4B). For all samples in the two series, the
277 resonance at approximately 65 ppm, corresponding to Al (IV), is much stronger than that
278 at around 9 ppm, corresponding to Al (VI) (Woessner 1989). This suggests that Al ions
279 prefer to occupy tetrahedral sites instead of octahedral ones.

280 To investigate occupancy priority of Al in octahedral and tetrahedral sites, the ratios of
281 Al(IV)/Al(VI) in the synthetic saponites were calculated by deconvolution of ^{27}Al MAS
282 NMR spectra (Table 1). Well crystallized synthetic saponites (e.g., SAP-I-5.43,
283 SAP-I-7.89, SAP-II-5.43 and SAP-II-7.89) showed a higher Al(IV)/Al(VI) ratio than
284 poorly crystallized synthetic samples and the maximum values were reached in
285 SAP-I-5.43 (Al(IV)/Al(VI) = 25.6) and SAP-II-5.43 (Al(IV)/Al(VI) = 25.3). It must be
286 noted that all the ^{27}Al MAS NMR spectra of the well crystallized samples (e.g.,
287 SAP-I-5.43, SAP-I-7.89, SAP-II-5.43 and SAP-II-7.89) showed very low intensity of
288 Al(VI) signals while the intensity of Al(IV) signal is comparable to that of the samples
289 with low crystallinity. This suggests that Al(IV)/Al(VI) ratio has a significant effect on
290 the crystallinity of the synthetic saponite i.e., Al occupancy in octahedral sites has a
291 negative effect on the crystallinity of the synthetic saponites.

292 The cation exchange capacities (CEC) of the synthetic saponites were determined and

293 shown in Table 1. With the substitutions of Al^{3+} for Si^{4+} and Al^{3+} for Mg^{2+} , the synthetic
294 saponites are negatively charged (Brigatti et al. 2006). It is noteworthy that those well
295 crystallized synthetic saponites had a relatively higher CEC value than other samples
296 (Table 1). The substitution of Al^{3+} for Si^{4+} in tetrahedral sheet will result in a negative
297 charge. However, there is two possible ways for substitution of Al^{3+} for Mg^{2+} in the
298 octahedral sheet, i.e., $1\text{Al}^{3+} \rightarrow 1\text{Mg}^{2+}$ (Suquet et al. 1981) and $2\text{Al}^{3+} + \text{vacancy} \rightarrow 3\text{Mg}^{2+}$
299 (Vogels et al. 2005b). The case of $1\text{Al}^{3+} \rightarrow 1\text{Mg}^{2+}$ will result in a positive charge in the
300 synthetic product whereas $2\text{Al}^{3+} + \text{vacancy} \rightarrow 3\text{Mg}^{2+}$ will not lead to any net charge.
301 From Table 1, we can find that the substituting Al^{3+} amount in the tetrahedral sheets
302 decreased with the increment of Si/Al ratio. This means that the CEC of the synthetic
303 saponites should also decrease with the increment of Si/Al ratio if substitution of Al^{3+} for
304 Mg^{2+} in the octahedral sheet occurred as $2\text{Al}^{3+} + \text{vacancy} \rightarrow 3\text{Mg}^{2+}$. But CEC
305 measurements showed that the saponites with both relatively high and low Si/Al ratio,
306 corresponding to poorly crystallized samples, had low CEC values. This suggests that
307 substitution of $1\text{Al}^{3+} \rightarrow 1\text{Mg}^{2+}$ in the octahedral sheets occurred in the saponite synthesis
308 (Bisio et al. 2008).

309 On the other hand, ^{29}Si CPMAS NMR spectra also provided complementary
310 evidences for Al occupancy (Figs. 4C and 4D). For the well crystallized synthetic
311 saponites, two well resolved ^{29}Si signals were recorded at approximately -95 and -91
312 ppm, corresponding to $\text{Q}^3 \text{Si}(0\text{Al})$ and $\text{Q}^3 \text{Si}(1\text{Al})$ ($\text{Q}^m(\text{nAl})$, Q^m ($m=0, 1, 2, 3, 4$) refers to
313 the polymerization state of Si, and nAl ($n \leq m$) to the number of Al in the next-nearest

314 neighbor tetrahedral position), respectively (Lipsicas et al. 1984). With an increase or
315 decrease of Si/Al ratio, the Q^3 Si(0Al) and Q^3 Si(1Al) signals merged into one broad
316 signal, reflecting a decrease of local structural ordering around Si atoms and crystallinity
317 of the synthetic saponites. This is in agreement with XRD and electron microscope
318 analysis results.

319 As shown by the ^{29}Si CPMAS NMR spectra, the synthetic saponites with high Si/Al
320 ratio (e.g., SAP-I-39.00) displayed two well resolved broad signals centered at ca. -94
321 and -85 ppm, respectively. The broad and asymmetric signal centered at ca. -94 ppm is
322 an overlap of Q^3 Si(0Al) signal at ca. -94 ppm and Q^3 Si(1Al) at ca. -91 ppm as indicated
323 by spectral deconvolution (Fig. 5). With a decrease of Si/Al ratio, a prominent shoulder at
324 ca. -91 ppm corresponding to Q^3 Si(1Al) occurred in the less negative side of the main
325 signal of Q^3 Si(0Al) centered at ca. -95 ppm. The two signals reached a best resolution in
326 SAP-I-5.43, SAP-I-7.89, SAP-II-5.43 and SAP-II-7.89, which are well crystallized as
327 indicated by XRD and SEM observation. When the Si/Al ratio was further decreased, the
328 resolution between Q^3 Si(0Al) and Q^3 Si(1Al) signals decreased and the Q^3 Si(1Al) signal
329 became more prominent than Q^3 Si(0Al). This can be well explained by the change of
330 chemical composition in the synthetic saponites. A decrease of Si/Al ratio reflects more
331 Al ions were incorporated into the saponite structure, resulting an increase of the Q^3
332 Si(1Al) signal intensity.

333 In the ^{29}Si CPMAS NMR spectra of all samples, a signal at $-84 - -86$ ppm was
334 recorded, which was attributed to Q^3 Si(2Al) in the previous studies (Lipsicas et al. 1984;

335 Delevoeye et al. 2003). Interestingly, this signal has never been reported for natural clay
336 minerals. Theoretically, the Q^3 Si(2Al) signal only occurs when the Si/Al ratio in the
337 tetrahedral sheet is less than 3:1. Hence, the relatively high intensity of the resonance
338 around -86 ppm in the synthetic saponites with high Si/Al ratio (e.g., SAP-I-39.00 and
339 SAP-I-14.50) is unlikely attributed to Q^3 Si(2Al) taking into account the low amount of
340 Al^{3+} and the very weak Q^3 Si(1Al) resonance. A most possible attribution of the signal at
341 ca. -86 ppm is to the Q^2 Si(OAl) present at the layer edges of clay minerals (Vogels et al.
342 2005b).

343 To elucidate the origin of the signal at ca. -86 ppm, the synthetic saponites were
344 grafted with APTES in a mixture of ethanol-water (75/25, v/v). The obtained ^{29}Si
345 CPMAS NMR spectra of the saponites and grafting products were shown in Figure 5.
346 The occurrence of T^3 and T^2 signals at ca. -67.2 and -57.7 ppm indicated a successful
347 loading of APTES on the saponites and condensation among APTES molecules. After
348 grafting saponites with silane, we can find that the intensity of the signal at ca. -86 ppm
349 decreased whereas those of Q^3 Si(0Al) and Q^3 Si(1Al) increased. If the signal at ca. -86
350 ppm corresponds to Q^3 Si(2Al), its intensity should be not decreased after the grafting
351 reaction. Hence, the decreased intensity of the signal at -86 ppm and increased intensity
352 of Q^3 Si(0Al) and Q^3 Si(1Al) signals strongly suggest that the Q^2 Si was transformed to
353 Q^3 Si when silane was chemically bonded with the Si atoms at the layer edges (Herrera et
354 al. 2004; Daniel et al. 2008). This indicates that the signal at ca. -86 ppm should be
355 attributed to Q^2 Si at the clay layer edges. As shown by TEM and SEM observations, the

356 synthetic saponites are composed of small layers/particles with a high aspect ratio. In this
357 case, the amount of Si atoms situated at the layer edges is relatively large and could be
358 detected by MAS NMR (Daniel et al. 2008). The general absence of the Q² Si resonance
359 in the ²⁹Si CPMAS NMR spectra of phyllosilicates may be ascribed to the large particle
360 size of naturally occurring samples (Vogels et al. 2005b).

361 In addition, we found that the intensity increase of Q³ Si(0Al) and Q³ Si(1Al) signals in
362 SAP-I-12.30-APTES and SAP-I-39.00-APTES was more prominent than that in
363 SAP-I-5.43-APTES. Only a slight intensity increase could be seen for
364 SAP-I-5.43-APTES attributed to the effect of particle size. As shown by SEM and TEM
365 images, SAP-I-5.43 displayed larger saponite layers when compared with SAP-I-12.30
366 and SAP-I-39.00. The higher aspect ratio of saponite in SAP-I-5.43 is a disadvantage for
367 successful silane grafting.

368 **ACKNOWLEDGEMENTS**

369 The authors thank Brian L. Phillips, J. Theo Kloprogge and the other two
370 anonymous reviewers for the helpful comments and reviews. This work was financially
371 supported by National Natural Science Foundation of China (Grant No. U0933003 and
372 41002015), National Key Technology R&D Program (Grant No. 2011BAB03B06).

373 **REFERENCES CITED**

- 374 Alexandre, M., and Dubois, P. (2000) Polymer-layered silicate nanocomposites:
375 preparation, properties and uses of a new class of materials. *Materials Science and*
376 *Engineering: R: Reports*, 28, 1-63.
- 377 Bisio, C., Gatti, G., Boccaleri, E., Marchese, L., Superti, G.B., Pastore, H.O., and
378 Thommes, M. (2008) Understanding physico-chemical properties of saponite
379 synthetic clays. *Microporous and Mesoporous Materials*, 107, 90-101.
- 380 Brigatti, M. F., Galan, E., Theng, B.K.G. (2006) Structures and mineralogy of clay
381 minerals, In F. Bergaya, B.K.G. Theng and G. Lagaly, Eds., *Handbook of Clay*
382 *Science*, p. 19-86. Elsevier, Amsterdam.
- 383 Casagrande, M., Storaro, L., Lenarda, M., and Rossini, S. (2005) Solid acid catalysts
384 from clays: Oligomerization of 1-pentene on Al-pillared smectites. *Catalysis*
385 *Communications*, 6, 568-572.
- 386 Costenaro, D., Gatti, G., Carniato, F., Paul, G., Bisio, C., Marchese, L. (2012) The effect of
387 synthesis gel dilution on the physico-chemical properties of acid saponite clays.
388 *Microporous and Mesoporous Materials*, 162, 159–167.
- 389 Daniel, L.M., Frost, R.L., and Zhu, H.Y. (2008) Edge-modification of laponite with
390 dimethyl-octylmethoxysilane. *Journal of Colloid and Interface Science*, 321,
391 302-309.
- 392 Delevoye, L., Robert, J.-L., and Grandjean, J. (2003) ^{23}Na 2D 3QMAS NMR and ^{29}Si ,
393 ^{27}Al MAS NMR investigation of laponite and synthetic saponites of variable

- 394 interlayer charge. *Clay Minerals*, 38(1), 63-69.
- 395 Farmer, V.C., Krishnamurti, G.S.R., and Huang, P.M. (1991) Synthetic allophane and
396 layer-silicate formation in SiO₂-Al₂O₃-FeO-Fe₂O₃-MgO-H₂O systems at 23°C and
397 89°C in a calcareous environment. *Clays and Clay Minerals*, 39, 561-570.
- 398 Farmer, V.C., Mchardy, W.J., Elsass, F., and M., R. (1994) hk-ordering in aluminous
399 nontronite and saponite synthesized near 90 °C: effects of synthesis conditions on
400 nontronite composition and ordering. *Clays and Clay Minerals*, 42, 180-186.
- 401 Giannelis, E.P., Krishnamoorti, R., and Manias, E. (1999) Polymer-silicate
402 nanocomposites: Model systems for confined polymers and polymer brushes.
403 *Advances in Polymer Science*, 138, 107-147.
- 404 Goto, A., and Tatsumi, Y. (1994) Quantitative analysis of rock samples by an X-ray
405 fluorescence spectrometer (I). *The Rigaku Journal*, 11, 40-59.
- 406 He, H.P., Frost, R.L., Deng, F., Zhu, J.X., Wen, X.Y., and Yuan, P. (2004) Conformation
407 of surfactant molecules in the interlayer of montmorillonite studied by C-13 MAS
408 NMR. *Clays and Clay Minerals*, 52, 350-356.
- 409 He, H.P., Duchet, J., Galy, J., Gerard, J.F. (2005) Grafting of swelling clay materials with
410 3-aminopropyltriethoxysilane. *Journal of Colloid and Interface Science*, 288,
411 171-176.
- 412 He, H.P., Ma, Y.H., Zhu, J.X., Yuan, P., Qing, Y.H. (2010) Organoclays prepared from
413 montmorillonites with different cation exchange capacity and surfactant
414 configuration. *Applied Clay Science*, 48, 67-72.

- 415 Herrera, N.N., Letoffe, J.M., Putaux, J.L., David, L., and Bourgeat-Lami, E. (2004)
416 Aqueous dispersions of silane-functionalized laponite clay platelets. A first step
417 toward the elaboration of water-based polymer/clay nanocomposites. *Langmuir*,
418 20, 1564-1571.
- 419 Higashi, S., Miki, H., and Komarneni, S. (2007) Mn-smectites: Hydrothermal synthesis
420 and characterization. *Applied Clay Science*, 38, 104-112.
- 421 Hu, X., Lu, G., and Yang, Y. (2000) Determination of cation exchange capacity in clay
422 $[\text{Co}(\text{NH}_3)_6]^{3+}$ exchange method. *Chinese Journal of Analytical Chemistry*, 28,
423 1402-1405.
- 424 Kawi, S., and Yao, Y.Z. (1999) Saponite catalysts with systematically varied Mg/Ni ratio:
425 synthesis, characterization, and catalysis. *Microporous and Mesoporous Materials*,
426 33, 49-59.
- 427 Kloprogge, J.T., Breukelaar, J., Jansen, J.B.H., and Geus, J.W. (1993) Development of
428 ammonium-saponites from gels with variable ammonium concentration and water
429 content at low-temperatures. *Clays and Clay Minerals*, 41, 103-110.
- 430 Kloprogge, J.T., Breukelaar, J., Geus, J.W., and Jansen, J.B.H. (1994a) Characterization
431 of Mg-saponites synthesized from gels containing amounts of Na^+ , K^+ , Rb^+ ,
432 Ca^{2+} , Ba^{2+} , or Ce^{4+} equivalent to the CEC of the saponite. *Clays and Clay*
433 *Minerals*, 42, 18-22.
- 434 Kloprogge, J.T., Breukelaar, J., Wilson, A.E., Geus, J.W., and Jansen, J.B.H. (1994b)
435 Solid-state nuclear magnetic resonance spectroscopy on synthetic

- 436 ammonium/aluminum-saponites. *Clays and Clay Minerals*, 42, 416-420.
- 437 Klopogge, J.T., Hickey, L., and Frost, R.L. (1999) Infrared study of some synthetic
438 saponites: Effect of NH_4/Al and $\text{H}_2\text{O}/(\text{Si}+\text{Al})$ ratios during the crystallization.
439 *Journal of Materials Science Letters*, 18, 1401-1403.
- 440 Lagaly, G. (1981) Characterization of clays by organic compounds. *Clay Minerals*, 16,
441 1-21.
- 442 Lipsicas, M., Raythatha, R.H., Pinnavaia, T.J., Johnson, I.D., Giese, R.F., Costanzo, P.M.,
443 and Robert, J.L. (1984) Silicon and aluminium site distributions in 2:1 layered
444 silicate clays. *Nature*, 309, 604-607.
- 445 Mackenzie, R.C. (1957) Saponite from Allt Ribhein, Fiskavaig Bay, Skye. *Mineralogical*
446 *Magazine*, 31, 672-680.
- 447 Moronta, A. (2004) Catalytic and adsorption properties of modified clay surfaces.
448 *Interface Science and Technology*, 1, 321-344.
- 449 Suquet, H., Malard, C., Copin, E., and Pezerat, H. (1981) Variation du parametre b et de
450 la distance basale d_{001} dans une serie de saponites a charge croissante: I. Etats
451 hydrates. *Clay Minerals*, 16, 53-67.
- 452 Utracki, L.A., Sepehr, M., and Boccaleri, E. (2007) Synthetic, layered nanoparticles for
453 polymeric nanocomposites (PNCs). *Polymers for Advanced Technologies*, 18,
454 1-37.
- 455 Varma, R.S. (2002) Clay and clay-supported reagents in organic synthesis. *Tetrahedron*,
456 58, 1235-1255.

- 457 Vicente, I., Salagre, P., Cesteros, Y., Medina, F., and Sueiras, J.E. (2010)
458 Microwave-assisted synthesis of saponite. *Applied Clay Science*, 48, 26-31.
- 459 Vicente Rodriguez, M.A., Suarez Barrios, M., Lopez Gonzalez, J.D., and Banares Munoz,
460 M.A. (1994) Acid activation of a ferrous saponite (griffithite); physico-chemical
461 characterization and surface area of the products obtained. *Clays and Clay*
462 *Minerals*, 42, 724-730.
- 463 Vogels, R.J.M.J., Breukelaar, J., Kloprogge, J.T., Jansen, J.B.H., and Geus, J.W. (1997)
464 Hydrothermal crystallization of ammonium-saponite at 200 °C and autogeneous
465 water pressure. *Clays and Clay Minerals*, 45, 1-7.
- 466 Vogels, R.J.M.J., Kloprogge, J.T., and Geus, J.W. (2005a) Catalytic activity of synthetic
467 saponite clays: effects of tetrahedral and octahedral composition. *Journal of*
468 *Catalysis*, 231, 443–452.
- 469 Vogels, R.J.M.J., Kloprogge, J.T., and Geus, J.W. (2005b) Synthesis and characterization
470 of saponite clays. *American Mineralogist*, 90, 931-944.
- 471 Woessner, D.E. (1989) Characterization of clay minerals by ²⁷Al nuclear magnetic
472 resonance spectroscopy. *American Mineralogist*, 74, 203–215.
- 473 Xue, S., and Pinnavaia, T.J. (2010) Methylene-functionalized saponite: A new type of
474 organoclay with CH₂ groups substituting for bridging oxygen centers in the
475 tetrahedral sheet. *Applied Clay Science*, 48, 60-66.
- 476 Yao, M., Liu, Z.Y., Wang, K.X., Zhu, M.Q., and Sun, H.J. (2005) Application of FTIR
477 technique in microwave-hydrothermal synthesis of saponite. *Spectroscopy and*

478 Spectral Analysis, 25, 870-873.

479 Zanetti, M., Lomakin, S., and Camino, G. (2000) Polymer layered silicate
480 nanocomposites. *Macromolecular Materials and Engineering*, 279, 1-9.

481 Zhang, D., Zhou, C.H., Lin, C.X., Tong, D.S., and Yu, W.H. (2010) Synthesis of clay
482 minerals. *Applied Clay Science*, 50, 1-11.

483

484 **Tables**

485

486 Table 1. The molar ratios of Si, Al and Mg in the starting materials, CEC and
 487 Al(IV)/Al(VI) ratios of the synthetic saponites.

	samples	Si:Al:Mg	Nominal Si/Al ^a	Measured Si/Al ^b	CEC ^c (mmol/100g)	Al(IV)/Al(VI) ^d	Al(IV) ^e (%)
Series I	SAP-I-1.80	2.57:1.43:3.00	1.80	1.8	108	3.9	25.1
	SAP-I-2.13	2.72:1.28:3.00	2.13	2.2	118	5.0	22.6
	SAP-I-2.33	2.80:1.20:3.00	2.33	2.3	104	5.6	22.2
	SAP-I-4.50	3.27:0.73:3.00	4.50	4.5	133	13.6	15.4
	SAP-I-5.43	3.38:0.63:3.00	5.43	5.6	133	25.6	13.7
	SAP-I-7.89	3.55:0.45:3.00	7.89	7.9	120	16.7	10.2
	SAP-I-12.30	3.70:0.30:3.00	12.30	12.4	117	8.9	6.8
	SAP-I-14.50	3.74:0.26:3.00	14.50	13.6	116	6.1	6.0
	SAP-I-39.00	3.90:0.10:3.00	39.00	33.9	113	4.0	2.2
Series II	SAP-II-1.80	2.72:1.53:3.00	1.80	1.9	113	5.2	24.8
	SAP-II-2.13	2.72:1.28:3.00	2.13	2.3	114	6.3	22.6
	SAP-II-2.33	2.72:1.17:3.00	2.33	3.3	135	8.8	19.1
	SAP-II-4.50	2.72:0.60:3.00	4.50	4.8	140	8.1	15.4
	SAP-II-5.43	2.72:0.50:3.00	5.43	7.5	125	25.3	10.8
	SAP-II-7.89	2.72:0.35:3.00	7.89	10.8	116	10.4	7.7
	SAP-II-12.30	2.72:0.22:3.00	12.30	15.3	116	5.1	6.1
	SAP-II-14.50	2.72:0.19:3.00	14.50	14.2	103	5.4	5.3
	SAP-II-39.00	2.72:0.22:3.00	39.00	43.7	115	2.5	1.8

488 **Notes:**

- 489 a: Nominal Si/Al ratio in the synthesis gel based on the chemical composition of the
 490 starting solutions for the synthesis.
- 491 b: Si/Al ratio in the synthetic saponites determined by XRF measurement, which has
 492 measurement errors within 5%.
- 493 c: Accuracy of the CEC measurement is within 5%.
- 494 d: Determined by deconvolution of ²⁷Al MAS NMR spectra with uncertainty of ±3%.
- 495 e: Calculated percentage of Al(IV)/[Al(IV)+Si] in tetrahedral sheet with uncertainty of
 496 ±5%.
- 497

498 **Figure captions**

499

500 **FIGURE 1** XRD patterns of synthetic saponites in Series I (left) with Si/Al molar ratio
501 of (a) 1.80, (b) 2.13, (c) 2.33, (d) 4.50, (e) 5.43, (f) 7.89, (g) 12.30, (h) 14.50 and (i) 39.00,
502 and in Series II (right) with Si/Al molar ratio of (a) 1.80, (b) 2.13, (c) 2.33, (d) 4.50, (e)
503 5.43, (f) 7.89, (g) 12.30, (h) 14.50, and (i) 39.00.

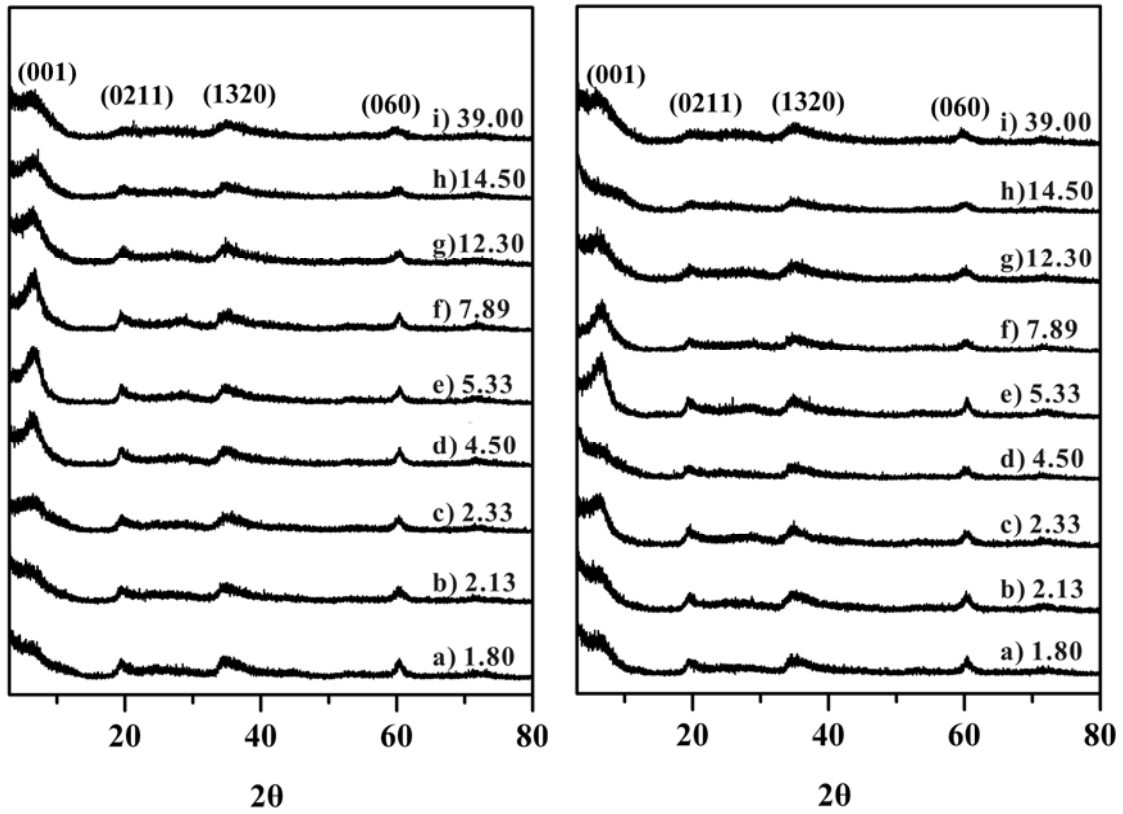
504 **FIGURE 2** SEM (a–d) and TEM (e, f) images of synthetic saponites: (a) SAP-I-2.33,
505 (b) SAP-I-5.43, (c) SAP-I-7.89, (d) SAP-I-39.00, (e) SAP-I-2.33, and (f) SAP-I-5.43.

506 **FIGURE 3** XRD patterns of (a) SAP-I-2.33 and (b) SAP-I-2.33-1CEC, (c) SAP-I-5.43
507 and (d) SAP-I-5.43-1CEC, (e) SAP-I-7.89 and (f) SAP-I-7.89-1CEC.

508 **FIGURE 4** ^{27}Al MAS NMR (A, B) and ^{29}Si CPMAS NMR (C, D) spectra of synthetic
509 saponites in Series I (A, C) with Si/Al molar ratio of (a) 1.80, (b) 2.13, (c) 2.33, (d) 4.50,
510 (e) 5.43, (f) 7.89, (g) 12.30, (h) 14.50 and (i) 39.00, and in Series II (B, D) with Si/Al
511 molar ratio of (a) 1.80, (b) 2.13, (c) 2.33, (d) 4.50, (e) 5.43, (f) 7.89, (g) 12.30, (h) 14.50,
512 and (i) 39.00.

513 **FIGURE 5** ^{29}Si CPMAS NMR spectra of (a) SAP-I-5.43 (dash line) and (b)
514 SAP-I-5.43-APTES (solid line), (c) deconvoluted spectrum of SAP-I-5.43 (dash dot line)
515 (d) SAP-I-12.30 (dash line), (e) SAP-I-12.30-APTES (solid line), (f) deconvoluted
516 spectrum of SAP-I-12.30 (dash dot line), (g) SAP-I-39.00 (dash line), (h)
517 SAP-I-39.00-APTES (solid line) and (i) deconvoluted spectrum of SAP-I-39.00 (dash dot
518 line).

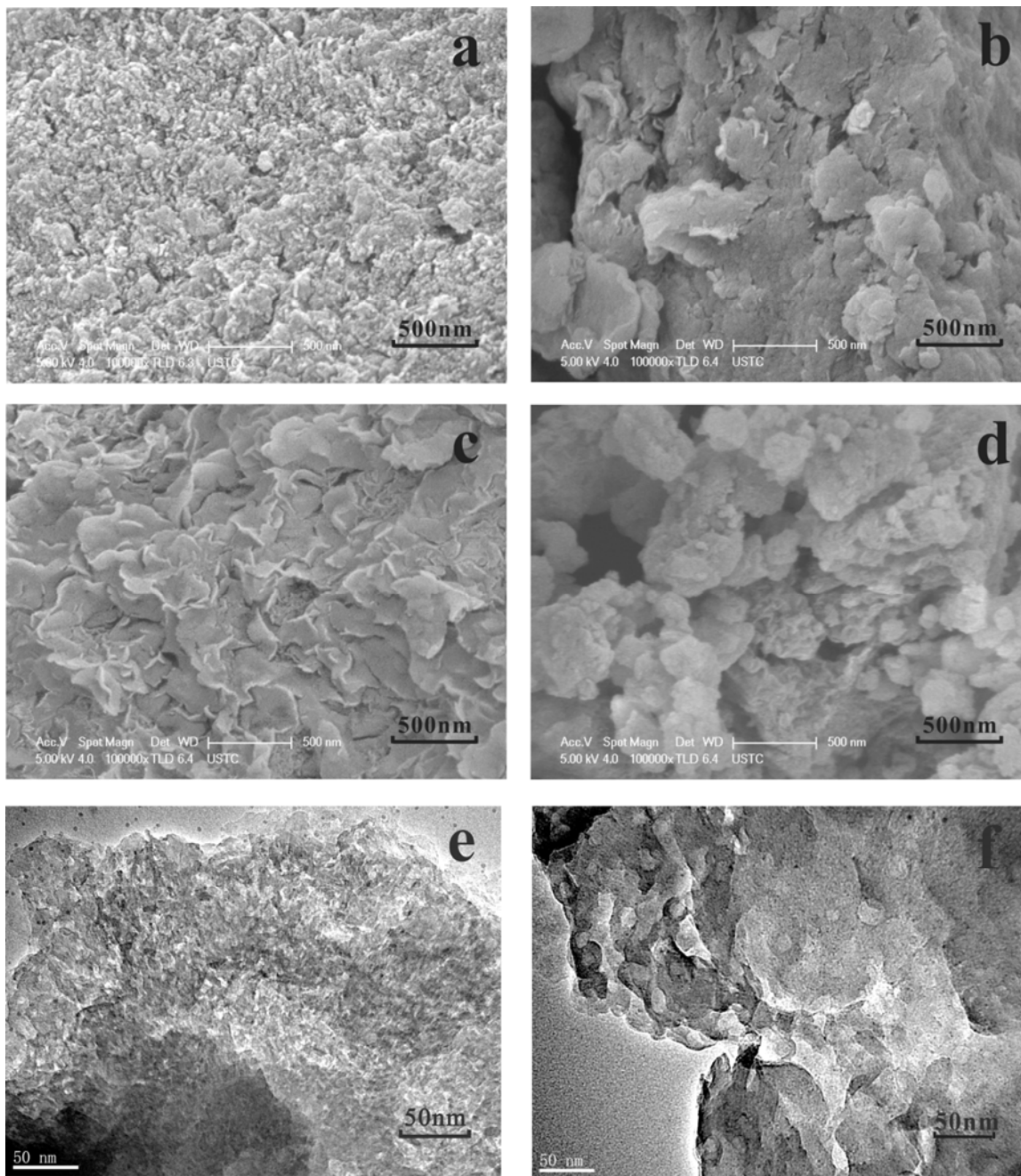
519 **FIGURE 1**



520

521 **FIGURE 2**

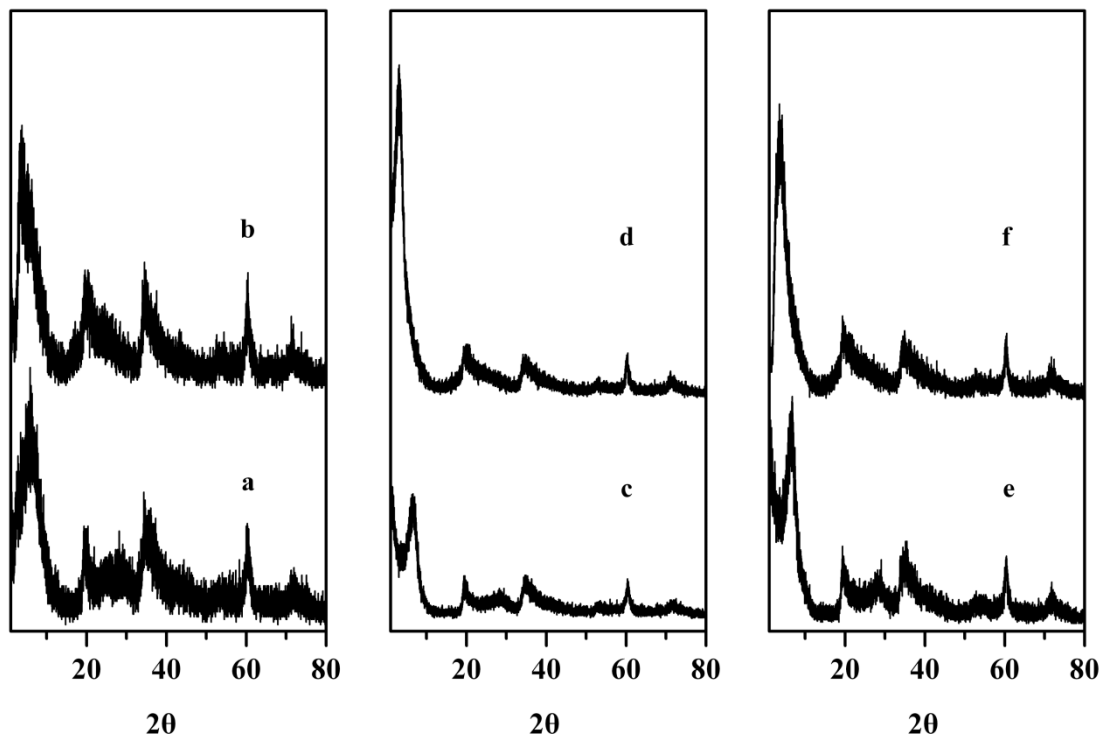
522



523

524

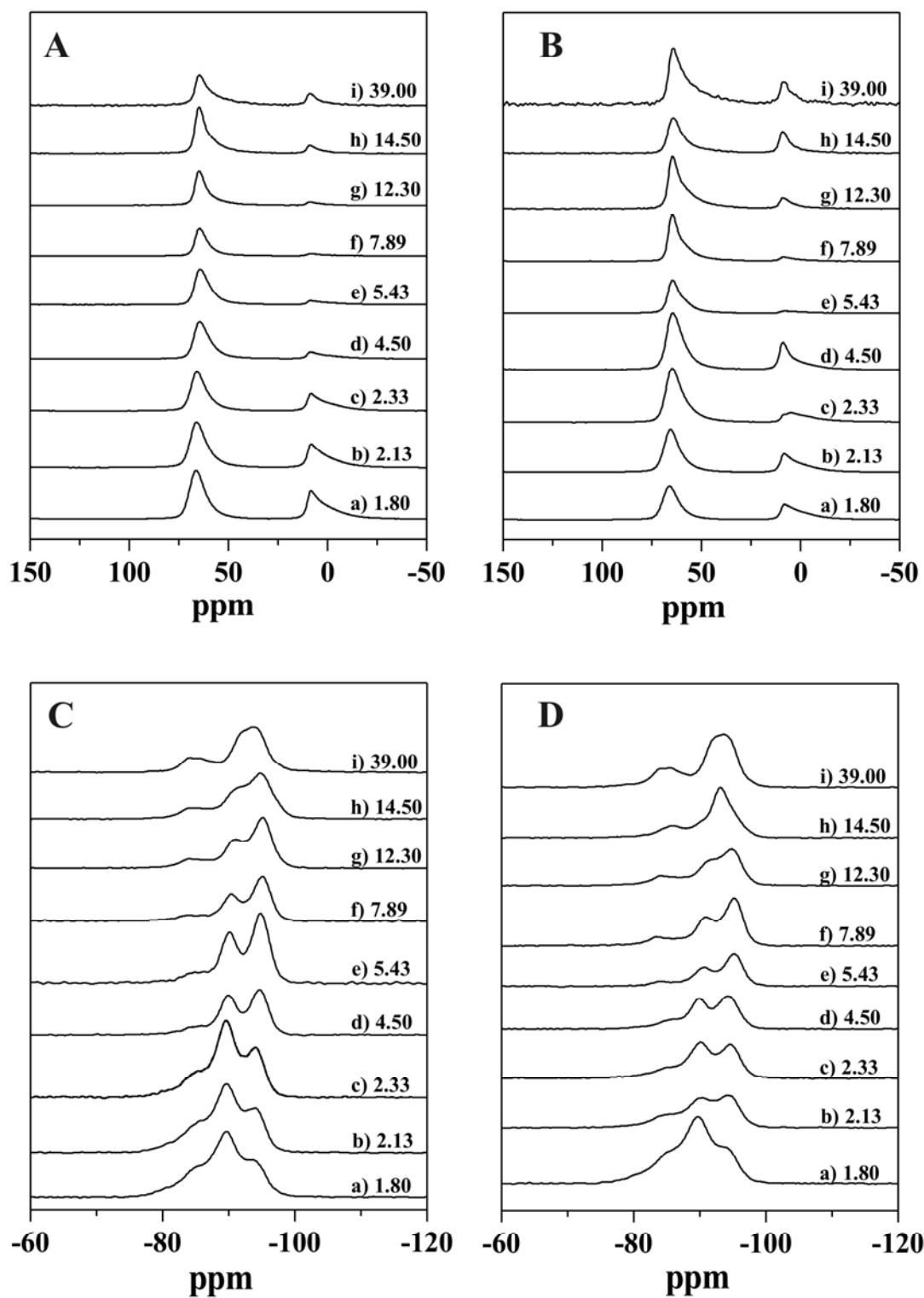
525



527

528

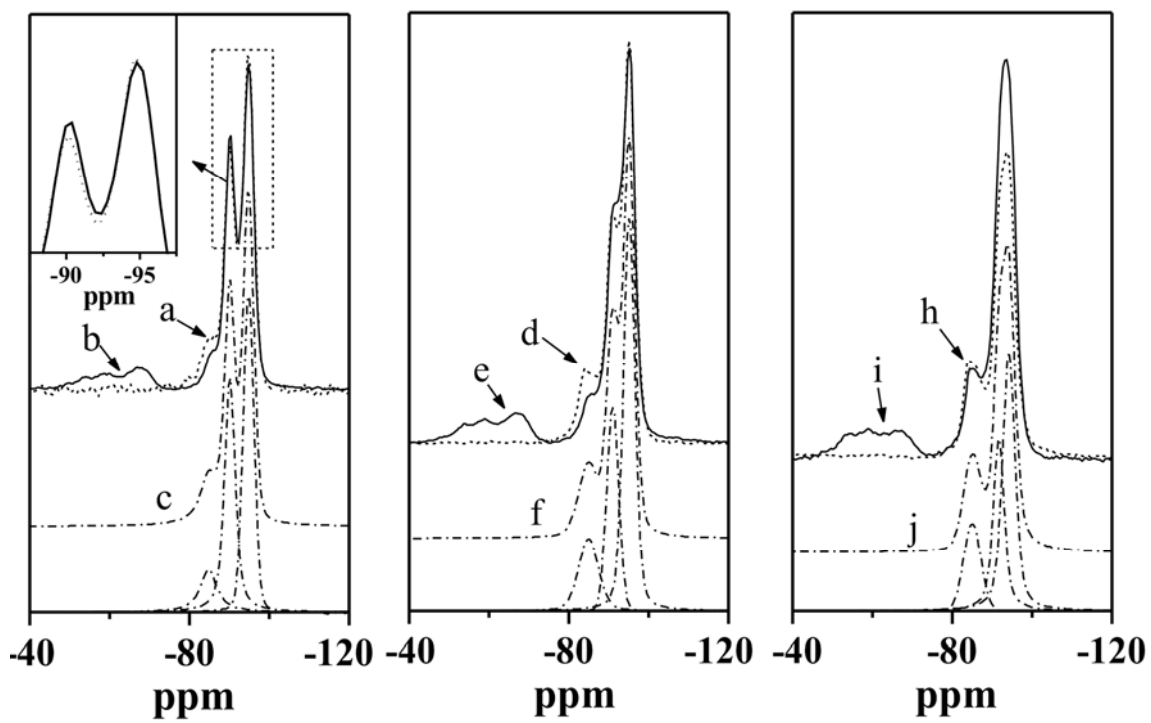
529 **FIGURE 4**
530



531
532

533 **FIGURE 5**

534



535

